

# Active robustness against the detuning-error for Rydberg quantum gates\*

Qing-Ling Hou<sup>1</sup>, Han Wang<sup>1,2</sup>, and Jing Qian<sup>1,3</sup>

<sup>1</sup>*State Key Laboratory of Precision Spectroscopy,  
Department of Physics, School of Physics and Electronic Science,  
East China Normal University, Shanghai, 200062, China*

<sup>2</sup>*Hong Kong University of Science and Technology, Guangzhou, 511453, China and*  
<sup>3</sup>*Shanghai Branch, Hefei National Laboratory, Shanghai 201315, China*

(Dated: April 19, 2024)

Error suppression to the experimental imperfections is a central challenge for useful quantum computing. Recent studies have shown the advantages of using single-modulated pulses based on optimal control which can realize high-fidelity two-qubit gates in neutral-atom arrays. However, typical optimization only minimizes the ideal gate error in the absence of any decay, which allows the gate to be passively influenced by all error sources leading to an exponential increase of sensitivity when the error becomes larger. In the present work, we propose the realization of two-qubit  $C_Z$  gates with *active* robustness against two-photon detuning errors. Our method depends on a modified cost function in numerical optimization for shaping gate pulses, which can minimize, not only the ideal gate error but also the fluctuations of gate infidelity over a wide error range. We introduce a family of Rydberg blockade gates with *active* robustness towards the impacts of versatile noise sources such as Doppler dephasing and ac Stark shifts. The resulting gates with robust pulses can significantly increase the insensitivity to any type of errors acting on the two-photon detuning, benefiting from a relaxed requirement of colder atomic temperatures or more stable lasers for current experimental technology.

## I. INTRODUCTION

The ability to achieve high-fidelity two-qubit quantum gates is a key task for large-scale quantum computing with trapped neutral atoms [1–4], while noises from versatile experimental imperfections will fundamentally limit the achievable gate fidelity [5], leading to a huge gap to other state-of-the-art platforms such as superconducting qubits, trapped ions, quantum dots and nuclear magnetic resonance systems [6–10]. Recent work has demonstrated that the execution of modulated pulses based on optimal control can realize high-fidelity entangling operations [11]. And to date the best reported two-qubit gate fidelity using optimal control and atomic dark state reaches  $\mathcal{F} = 0.995$  [12]. The optimal control technique enables a smooth modulation of the laser amplitude or phase in time without the requirement for individual addressability of atoms [13–18]. This outperforms the original  $\pi$ -gap- $\pi$  method [19–21] by suppressing severe decoherence between the ground and Rydberg states [21–23].

The typical optimization focuses on minimizing the ideal gate infidelity in the absence of any noise. *e.g.* A time-optimal gate contains the merit of minimizing the gate duration together with a smaller time-spent in the Rydberg state which makes the gate robust to intrinsic Rydberg decay error [24]. Whereas other technical errors will passively affect the gate performance suggesting the necessity of subsequent error correction methods regardless of the system [25–30]. Recently, performing low-error quantum gates with noise-robust optimization has become an exciting frontier. To alleviate the sensitivity

of gates to type of errors that occur, *e.g.* constructing a specific cost function that possess optimal robustness with respect to some errors, is more attractive [31–33]. Via utilizing quantum optimal control with GRAPE algorithm [34] a family of Rydberg blockade gates with significantly improved performance is presented that can be simultaneously robust against the amplitude inhomogeneity and Doppler shifts [35]. Although these works may open unique opportunities for noise-robust quantum computing with atomic qubits, preserving an *active* robustness of systems to type of errors for Rydberg gates is still a big challenge.

In this work, we present the realization of two-qubit Rydberg  $C_Z$  gates with *active* robustness to all errors associated with the variation in two-photon detuning [37, 38]. To implement the noise-robust optimization, we mainly modify the cost function in the numerical Genetic algorithm which minimizes not only the ideal gate error but also the infidelity fluctuation over a wide error range, allowing the optimal pulse to be *actively* robust against the variation of errors. In addition, we adopt a realistic model by considering a native two-photon transition using adiabatic double-STIRAP pulse [39] which has shown a better robustness to the variation of experimental parameters such as laser amplitude and pulse shape [40–42]. To characterize the resulting two-qubit  $C_Z$  gates, we comparably exploit the results from typical and noise-robust optimizations. The latter can produce experimentally realizable pulses that are more robust to the variation of two-photon detunings caused by Doppler dephasing from finite atomic temperature [43] and ac Stark shifts [44, 45]. Our approach can be generalized to other type of errors paving the avenue for realizing noise-robust quantum gates in future experiments.

Finally we admit that there are two main weakness of

\* [jqian1982@gmail.com](mailto:jqian1982@gmail.com)

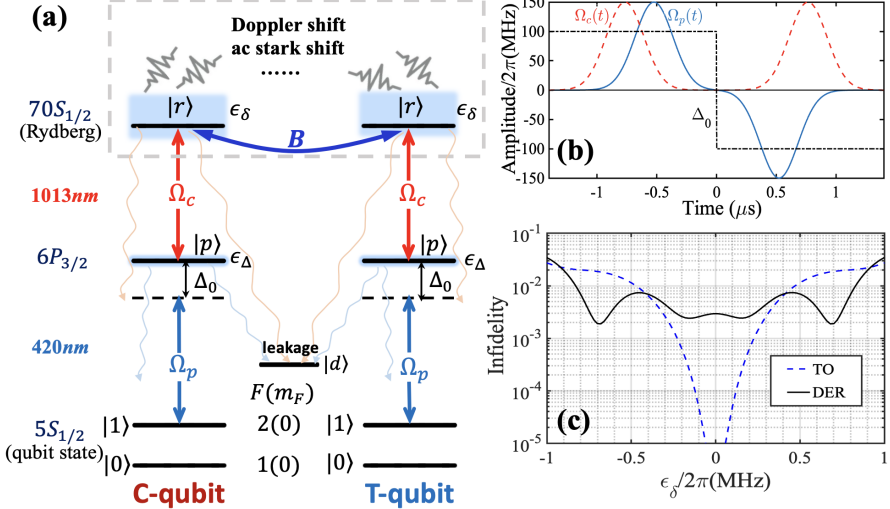


FIG. 1. Two-qubit  $C_Z$  gate protocol. (a) Atom-level diagram. Qubits are encoded in two hyperfine clock states  $|0\rangle$  and  $|1\rangle$  of  $^{87}\text{Rb}$  atoms. Atomic excitation to the Rydberg state  $|r\rangle$  is carried out by a two-photon transition via a largely-detuned intermediate state  $|p\rangle$  (detuned by  $\Delta_0$ ), driven by 420 nm and 1013 nm lasers.  $|d\rangle$  is a leakage state that collects most of the spontaneous decays from  $|p\rangle$  and  $|r\rangle$  except returning to  $|0\rangle$  and  $|1\rangle$ . The branching ratios used for different scattering rates are:  $b_{r\rightarrow 0} = 0.059$ ,  $b_{r\rightarrow 1} = 0.055$ ,  $b_{r\rightarrow d} = 0.886$ , and  $b_{p\rightarrow 0} = 0.1354$ ,  $b_{p\rightarrow 1} = 0.2504$ ,  $b_{p\rightarrow d} = 0.6142$ , together with a  $1/\gamma_r = 375 \mu\text{s}$  lifetime for  $|r\rangle$  and a  $1/\gamma_p = 0.118 \mu\text{s}$  lifetime for  $|p\rangle$ , chosen from [36]. The van der Waals interaction leads to a large energy shift  $B$  if both atoms are in  $|r\rangle$  preventing their simultaneous excitation in the Rydberg blockade limit.  $\epsilon_\Delta$  and  $\epsilon_\delta$  represent unknown detuning errors respectively to the intermediate and Rydberg states possibly from versatile experimental imperfections. (b) The pulse sequence  $\Omega_p(t)$ ,  $\Omega_c(t)$  and the non-fluctuated intermediate detuning  $\Delta_0$ . Note that  $\Delta_0$  is switched between two STIRAP pulses. (c) The gate infidelity  $1 - \mathcal{F}_{\text{der(to)}}$  in the absence of spontaneous decay as a function of the two-photon detuning error  $\epsilon_\delta$ , given by the DER and TO pulses.

this protocol. First, the modified cost function contains two competing terms that means the improvement of robustness should be at the expense of a high ideal gate fidelity (see Appendix B). For a noise-robust pulse, we achieve the gate with an ideal fidelity of  $\mathcal{F} = 0.9971$ . Second, the proposed gates will be affected by other error sources not associated to the two-photon detuning. As compared to the typical-optimal pulse, our pulses are not explicitly robust to those errors. Especially due to the use of an adiabatic pulse that elongates the gate duration, our scheme is more susceptible to the fluctuation in laser phase [46, 47].

## II. MODEL DESCRIPTION AND HAMILTONIAN

Consider a level scheme for two-qubit  $C_Z$  gates, as shown in Fig.1(a). Each atom is modeled as a native four-level system with long-lived hyperfine qubit states  $|0\rangle, |1\rangle$ , an intermediate state  $|p\rangle$  and an uppermost Rydberg state  $|r\rangle$  [48]. The coherent excitation from  $|1\rangle$  to  $|r\rangle$  is mediated by a resonant two-photon transition with laser Rabi frequencies  $\Omega_p, \Omega_c$ , largely detuned by  $\Delta_0$  from the intermediate state  $|p\rangle$ , *i.e.*  $|\Delta_0| \gg \Omega_p, \Omega_c$ . We assume a strong Rydberg blockade condition where two atoms trapped in two optical tweezers [49] with a distance smaller than the blockade radius, can bring a

strong energy shift  $B$  to prevent simultaneous excitation of both atoms [51, 52].

The total Hamiltonian governing the dynamics of the system, reads

$$\hat{H} = \hat{H}_c \otimes \hat{I} + \hat{I} \otimes \hat{H}_t + B|r r\rangle\langle r r| \quad (1)$$

with

$$\begin{aligned} \hat{H}_{j \in (c,t)} = & \frac{\Omega_p}{2}|p\rangle_j\langle 1| + \frac{\Omega_c}{2}|r\rangle_j\langle p| + \text{H.c.} - \epsilon_\delta|r\rangle_j\langle r| \\ & - (\Delta_0 + \epsilon_\Delta)|p\rangle_j\langle p| \end{aligned} \quad (2)$$

for single control or target qubit. Here,  $\epsilon_\Delta$  and  $\epsilon_\delta$  treats as the unknown yet constant detuning error over the gate duration possibly caused by versatile noise sources such as atomic velocity and laser fluctuations. We point out that, the intermediate detuning error  $\epsilon_\Delta$  is less important because  $|\Delta_0| \gg \epsilon_\Delta$  arising a negligible impact  $10^{-9} \sim 10^{-6}$  on fidelity(see Appendix C) [53]. Nevertheless, the laser frequency is resonant with the two-photon transition between  $|1\rangle$  and  $|r\rangle$ , making the role of two-photon detuning error  $\epsilon_\delta$  more crucial in the scheme.

### III. ACTIVE-ROBUSTNESS TWO-QUBIT $C_Z$ GATES

#### A. Double STIRAP pulse sequences

We proceed by describing the implementation of specific pulse sequences that result in a  $\pi$ -phase( $C_Z$ ) gate. The requirement for a universal controlled-phase gate is that the laser pulses  $\Omega_{p,c}(t)$  and the detuning  $\Delta_0$  (in the absence of any error) are applied such that states  $|01\rangle$ ,  $|10\rangle$ ,  $|11\rangle$  return to their ground states with phases  $\phi_{01}$ ,  $\phi_{10}$ ,  $\phi_{11}$ , in which  $\phi_{01} = \phi_{10}$  by symmetry. The  $C_Z$  gate is realized for  $\phi_{11} = 2\phi_{01} - \pi$  [54]. To realize this gate, we resort to the protocol using double sequences of adiabatic STIRAP pulse which provides strongly suppressed insensitivity to the fluctuations in laser amplitude [55]. The adiabatic pulses are given by

$$\Omega_p(t) = \Omega_p^{\max} (e^{-\frac{(t+t_1)^2}{2\omega^2}} - e^{-\frac{(t-t_1)^2}{2\omega^2}}) \quad (3)$$

$$\Omega_c(t) = \Omega_c^{\max} (e^{-\frac{(t+t_2)^2}{2\omega^2}} + e^{-\frac{(t-t_2)^2}{2\omega^2}}) \quad (4)$$

with  $\Omega_{p,c}^{\max}$ ,  $t_{1,2}$ ,  $\omega$  the peak amplitude, the pulse center and the pulse width, respectively. Note that, in addition to the phase change of  $\Omega_p(t)$  by  $\pi$  in the second STIRAP sequence, the sign of intermediate detuning  $\Delta_0$  is also reversed in the middle of the gate [56], as shown in Fig.1(b).

To understand the reason of this pulse(detuning) reversion, we demonstrate the physics associated with a single three-level system  $\{|1\rangle, |p\rangle, |r\rangle\}$  at which the Hamiltonian is readily given by (equivalent to Eq.2 without detuning errors  $\epsilon_\Delta, \epsilon_\delta$ )

$$\hat{H} = \begin{bmatrix} 0 & \frac{\Omega_p}{2} & 0 \\ \frac{\Omega_p}{2} & -\Delta_0 & \frac{\Omega_c}{2} \\ 0 & \frac{\Omega_c}{2} & 0 \end{bmatrix} \quad (5)$$

At large intermediate detuning  $|\Delta_0| \gg \Omega_{p,c}^{\max}$ , the system is conveniently described by one adiabatic dark state  $|d\rangle$  and two bright states  $|+\rangle, |-\rangle$ , which are

$$\begin{aligned} |d\rangle &= -\frac{1}{\sqrt{1+\alpha^2}}|1\rangle + \frac{\alpha}{\sqrt{1+\alpha^2}}|r\rangle \\ |+\rangle &= \frac{\alpha}{\sqrt{1+\alpha^2}}|1\rangle + \frac{\sqrt{1+\alpha^2}\Omega_c}{2\Delta_0}|p\rangle + \frac{1}{\sqrt{1+\alpha^2}}|r\rangle \\ |-\rangle &= -\frac{\alpha\Omega_c}{2\Delta_0}|1\rangle + |p\rangle - \frac{\Omega_c}{2\Delta_0}|r\rangle \end{aligned} \quad (6)$$

with the corresponding eigenvalues  $\lambda_d = 0$ ,  $\lambda_+ \approx \frac{(1+\alpha^2)}{4\Delta_0}$ ,  $\lambda_- \approx -\Delta_0$  to the leading order in  $\frac{(1+\alpha^2)\Omega_c^2}{\Delta_0^2}$  where  $\alpha = \Omega_p/\Omega_c$ . Reversing the sign of intermediate detuning  $\Delta_0 \rightarrow -\Delta_0$  can make the accumulated dynamical phase vanish due to  $\int_{-T_g/2}^{T_g/2} \lambda_{d,+,-} dt = 0$  ( $T_g$  is the gate duration). Then an additional geometric phase [57] arises owing to the relative phase switching between  $\Omega_p$  and

$\Omega_c$  which gives an extra  $\pi$  phase difference between  $|1\rangle$  and  $|r\rangle$  because of  $\alpha \rightarrow -\alpha$  in the second STIRAP sequence [58]. Such pulse inversion can finally result in the state evolution obeying  $|01\rangle \rightarrow -|0r\rangle \rightarrow -|01\rangle$ ,  $|10\rangle \rightarrow -|r0\rangle \rightarrow -|10\rangle$  so  $\phi_{01} = \phi_{10} = \pi$ . The  $|11\rangle$  state evolves within the Rydberg blockade regime as an effective two-level system by following  $|11\rangle \rightarrow -\frac{|1r\rangle+|r1\rangle}{\sqrt{2}} \rightarrow -|11\rangle$  and also accumulates  $\phi_{11} = \pi$ , which realizes the  $C_Z$  gate due to  $\phi_{11} = -\pi + \phi_{01} + \phi_{10}$ . The derivation for the effective couplings and numerical verification of the gate can be found in Appendix A.

#### B. Method for numerical calculation

The  $C_Z$  gate performance is quantified by the gate fidelity. For any input state  $|\Psi_j\rangle \in \{|00\rangle, |01\rangle, |10\rangle, |11\rangle\}$  ( $j = 1, \dots, 4$ ), the initial matrix can be expressed as

$$\hat{\rho}_{in} = |\Psi_j\rangle\langle\Psi_j| \quad (7)$$

and its dynamical evolution  $\hat{\rho}(t)$  can be analyzed by numerical integration of the two-atom master equation in the Lindblad form [59]

$$\frac{\partial \hat{\rho}}{\partial t} = -i[\hat{H}, \hat{\rho}] + \hat{\mathcal{L}}[\hat{\rho}] \quad (8)$$

where the Lindblad decay term is

$$\hat{\mathcal{L}}[\hat{\rho}] = \sum_{l \in \{c,t\}} \sum_{j \in \{p,r\}} \sum_{i \in \{0,1,d\}} \hat{\mathcal{L}}_{ij}^l \hat{\rho} \hat{\mathcal{L}}_{ij}^{l\dagger} - \frac{1}{2} \{ \hat{\mathcal{L}}_{ij}^{l\dagger} \hat{\mathcal{L}}_{ij}^l, \hat{\rho} \} \quad (9)$$

with jump operators  $\hat{\mathcal{L}}_{ij}^l = \sqrt{\gamma_j b_{j \rightarrow i}} |i\rangle\langle j|$  corresponding to the spontaneous decay from state  $|j\rangle$  with rate  $\gamma_j$  and branching ratio  $b_{j \rightarrow i}$  [60]. The uncoupled state  $|d\rangle$  represents all hyperfine ground states outside the qubit basis and all population leakage into  $|d\rangle$  is an uncorrectable error [61].

At  $t = T_g$ , the final density matrix is defined by  $\hat{\rho}_{out} = |\Psi_{T_g}\rangle\langle\Psi_{T_g}|$ , for each input  $\hat{\rho}_{in}$ , resulting in an element fidelity as

$$\mathcal{F}_j = \langle \Psi_j(T_g) | \hat{\rho}_{out} | \Psi_j(T_g) \rangle \quad (10)$$

which composes the realistic measurable truth table

$$\bar{\rho} = \begin{bmatrix} \mathcal{F}_1 & & & \\ & \mathcal{F}_2 & & \\ & & \mathcal{F}_3 & \\ & & & \mathcal{F}_4 \end{bmatrix} \quad (11)$$

The fidelity of the  $C_Z$  gate is given by

$$\mathcal{F} = \frac{1}{4} \text{Tr}[\sqrt{\hat{U}} \bar{\rho} \sqrt{\hat{U}}]^{1/2} \quad (12)$$

with the standard transformation matrix for a two-qubit  $C_Z$  gate

$$\hat{U} = \begin{bmatrix} 1 & & & \\ & -1 & & \\ & & -1 & \\ & & & -1 \end{bmatrix} \quad (13)$$

### C. Pulse optimization towards active robustness

To show a family of Rydberg quantum gates that are *actively* robust against any detuning error  $\epsilon_\delta \neq 0$ , we start by finding optimal STIRAP pulses  $\Omega_p(t), \Omega_c(t)$  for a two-qubit  $C_Z$  gate. Here we optimize the gate pulse to be detuning-error robust by employing the prior Genetic algorithm [62] yet containing a cleverly-chosen cost function,

$$J_{der} = [1 - \mathcal{F}(\epsilon_\delta = 0)]^2 + [\mathcal{F}_{\max}(\epsilon_\delta) - \mathcal{F}_{\min}(\epsilon_\delta)]^2 \quad (14)$$

Via minimizing this single-objective cost function  $J_{der}$  over a range of  $\epsilon_\delta \in [-\epsilon_0, \epsilon_0]$ , we observe that, not only the ideal gate error at  $\epsilon_\delta = 0$  is minimized, but also the sensitivity of the gate fidelity due to the change of  $\epsilon_\delta$  is significantly reduced, so-called the detuning-error robust(DER) pulse. It is worth emphasizing that such DER pulse has an *active* robustness to any magnitude of the two-photon detuning error as long as  $|\epsilon_\delta| < \epsilon_0$ . However, remember the typical-optimal(TO) pulse only minimizes the ideal gate infidelity in the absence of any error by letting the cost function as

$$J_{to} = 1 - \mathcal{F}(\epsilon_\delta = 0). \quad (15)$$

So any deviation  $\epsilon_\delta \neq 0$  can lead to an exponential increase of infidelity[see Fig.1(c)], in good agreement with Fig.2 of Ref.[35].

To our knowledge the achievable gate fidelity is fundamentally limited by the peak amplitude  $\Omega_{p,c}^{\max}$  which also sets a timescale for the gate duration  $T_g$ . Here we fix  $\Omega_{p,c}^{\max}/2\pi = 150$  MHz, maintaining a high two-photon Rabi frequency  $\Omega/2\pi = 5.625$  MHz, which restricts  $T_g$  to be about  $2.0 \mu\text{s}$  ensured by a minimal pulse area for qubit rotation [63]. Other parameters  $\Delta_0/2\pi = 2.0$  GHz,  $B/2\pi = 2.0$  GHz are fixed for simplicity. That leaves a few gate parameters  $(t_1, t_2, \omega)$  to be optimized. To find the DER pulse, we first minimize the cost function  $J_{der}$  using a reasonable range for denoting detuning deviation  $\epsilon_0/2\pi = 0.8$  MHz. This realizes an exact  $C_Z$  gate under optimal pulse parameters

$$t_1 = 0.6664\mu\text{s}, t_2 = 0.9260\mu\text{s}, \omega = 0.1666\mu\text{s}$$

While the gate parameters for a TO pulse are

$$t_1 = 0.4444\mu\text{s}, t_2 = 0.9027\mu\text{s}, \omega = 0.1587\mu\text{s}$$

in which the total gate duration is  $T_g = 2(t_2 + 3\omega) = (2.8517, 2.3259) \mu\text{s}$ , a slightly longer due to the use of adiabatic STIRAP pulses. We ignore the intermediate and Rydberg decays by  $\gamma_{p,r} = 0$  in the optimization and focus on the robustness of the gate pulse against detuning deviation  $\epsilon_\delta$ .

The gate infidelities  $1 - \mathcal{F}_{der(to)}$  are displayed in Fig.1(c) by the black-solid(DER) and blue-dashed(TO) lines. It is clear that the TO pulse depending on perfect optimization, benefits from a minimal value  $\sim 10^{-6}$  only if  $\epsilon_\delta$  is very small while the infidelity numbers increase

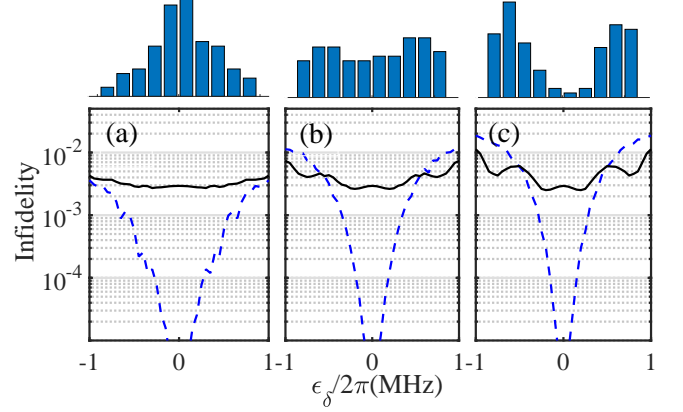


FIG. 2. The infidelity of the DER(black-solid), TO(blue-dashed) pulses under different noise sources. From (a) to (c), for each  $\epsilon_\delta$ , the real sampling numbers are randomly distributed within the range of  $[-\epsilon_\delta, \epsilon_\delta]$ , satisfying Gaussian, Uniform and U-shaped distributions with respective profiles shown on the top. Each point represents an average over 500 random samplings. No spontaneous decay is considered in the calculation.

exponentially with  $\epsilon_\delta$  as expected. For a large value of  $|\epsilon_\delta|/2\pi = 1.0$  MHz the infidelity reaches  $\sim 0.02$ . In contrast, the insensitivity of the DER pulse to the variation of  $\epsilon_\delta$  is greatly improved although the exact infidelity numbers stay at a relatively high level  $10^{-3} \sim 10^{-2}$ , yet its robustness is greatly enhanced. The DER pulse for  $|\epsilon_\delta|/2\pi = 0.7$  MHz has an infidelity of 0.0019, smaller than the TO pulse by one order of magnitude. Therefore, the DER optimization has appealing advantages in reducing the sensitivity of gate to the detuning deviation, especially for a larger  $\epsilon_\delta$  the predicted fidelity limit is still above 0.99. This improvement should be at the expense of a high ideal gate fidelity  $\mathcal{F}(\epsilon_\delta = 0) \sim 99.71\%$ (compared to 99.9996% for the TO pulse) because the choice of cost function  $J_{der}$  has incorporated the impact of two competing terms (see Appendix B).

Consequently the DER pulse protocol with *active* robustness will manifest a more dominant merit when the two-photon detuning deviation  $\epsilon_\delta$  is large. In this case the desirable gate implementation can be made more insensitive to any magnitude of detuning errors, maintaining a stable output performance.

### IV. DER PULSE UNDER DIFFERENT NOISE SOURCES

Accounting for the fact that the realistic detuning error induced by versatile experimental imperfections is unknown, so without loss of generality, we choose three different representations of the error distributions: Gaussian, Uniform, U-shaped, respectively for low, middle and high noise sources. The infidelity is shown as a function of detuning error  $\epsilon_\delta$  in Fig.2 with same set of optimal

pulse parameters(see Sec. III.C). By varying  $\epsilon_\delta$ , for a certain value, the realistic error number for single sampling is randomly obtained from a specific error function (top) and here we display the average result after significant samplings.

Seen from Fig.2(a-c), the DER pulse always has a reduced sensitivity to the variation of  $\epsilon_\delta$  no matter what the noise distribution is; while the TO pulse is very sensitive to  $\epsilon_\delta$ . This is expected because the DER pulse has exhibited the ability to overcome the influence from detuning deviation resulting in an improved robustness at the expense of high gate fidelities. However, we verify that, when the noise is relatively low forming as a Gaussian distribution the DER pulse has no advantages as compared to the TO pulse because it sustains a poor infidelity number above  $10^{-3}$  as  $\epsilon_\delta$  varies. While the DER pulse is a better choice when the detuning noise is large. By applying the Uniform or the U-shaped noise distributions, we clearly find the DER pulse always outperforms the TO pulse when  $|\epsilon_\delta|/2\pi > 0.5$  MHz. Therefore we remark that under a strong noise environment [64], the DER pulse protocol can outperform the TO protocol by exhibiting a more steady output with *active* robustness. An acceptable gate fidelity value above 0.99 remains attainable for a large detuning error.

## V. POTENTIAL APPLICATIONS TO REALISTIC NOISES

In a realistic experiment, two common major error sources that severely limit the fidelity of quantum gate operations, are the finite atom temperature [65] and the laser amplitude noise [66]. The former causes significant motional dephasing of the ground-Rydberg transitions. And the latter not only leads to fluctuated Rabi frequencies, but will also affect the two-photon detuning by inducing ac Stark shifts [67]. Especially for gate schemes relying on the optimal control of pulse shapes this laser-amplitude derivation(the latter) can significantly affect the observed gate fidelity [68, 69]. Here we have developed the appealing gates with *active* robustness to the errors associated with the variation in two-photon detuning. That means the gates are more robust against any type of errors which has an effect on the two-photon detuning. Other technical imperfections that passively influence the gate performance are analyzed in Appendix C.

### A. Doppler dephasing effect

So far the atomic thermal motion-induced Doppler dephasing is the most dominant error source in experiment, which ultimately limits the gate performance [70]. Atoms, whether they are warm or cold, are not stationary in the trap. The random velocity of the trapped atoms would lead to dephasing of ground-Rydberg excitation,

manifested as a modification to the phase of laser Rabi frequencies  $\Omega_p$  and  $\Omega_c$ , denoted by [71]

$$\Omega_p(t) \rightarrow \Omega_p(t)e^{i\epsilon_{\delta_p}t}, \Omega_c(t) \rightarrow \Omega_c(t)e^{i\epsilon_{\delta_c}t} \quad (16)$$

where  $\epsilon_{\delta_{p(c)}} = \vec{k}_{p(c)} \cdot \vec{v}$  is the Doppler shift with  $\vec{k}_{p,c}$  two participating laser wavevectors and  $\vec{v}$  the atomic random velocity extracted from a Gaussian distribution with standard deviation  $v_{rms} = \sqrt{k_B T/m}$  [72], where  $T$  is the temperature and  $m$  is the mass of atoms. Here we choose the laser wavelengths for the two-photon transition are, respectively,  $\lambda_p = 420$  nm and  $\lambda_c = 1013$  nm[see Fig.1(a)]. In order to diminish the Doppler dephasing, we use counterpropagating lasers instead of orthogonal ones which gives a minimal two-photon wavevector  $k_{eff} = 2\pi(1/\lambda_p - 1/\lambda_c) = 8.76 \times 10^6$  m<sup>-1</sup>. For a finite temperature  $T$ , this modification of laser phase equivalently means the realistic detuning fluctuation of excitation lasers felt by the atoms is a random variable which are  $\epsilon_\Delta = \epsilon_{\delta_p} = k_p v$  and  $\epsilon_\delta = \epsilon_{\delta_p} - \epsilon_{\delta_c} = k_{eff} v$ .

Remember in Sec.IV, we verify that the DER pulse has more promising advantages when the detuning error is large, especially for Uniform and U-shaped noise distributions. As the Doppler shift follows a standard Gaussian distribution, we improve the cost function replaced by  $J_{der-i}$  in the numerical optimization, towards the target of enhancing its dependence on the choice of noise type.

$$J_{der-i} = [1 - \mathcal{F}(\epsilon_\delta = 0)]^2 + [1 - \bar{\mathcal{F}}(\epsilon_\delta)]^2 \quad (17)$$

The first term in Eq.(17) suggests maximizing the ideal gate fidelity in the absence of any noise, same as  $J_{der}$ . While the second term means the average gate fidelity  $\bar{\mathcal{F}}(\epsilon_\delta)$  should be simultaneously maximized, where

$$\bar{\mathcal{F}}(\epsilon_\delta) = \frac{\mathcal{F}(\epsilon_{\delta 1})\omega_1 + \mathcal{F}(\epsilon_{\delta 2})\omega_2 + \dots + \mathcal{F}(\epsilon_{\delta n})\omega_n}{\omega_1 + \omega_2 + \dots + \omega_n} \quad (18)$$

with variables  $\epsilon_{\delta i}$  uniformly extracted from  $[-\epsilon_0, \epsilon_0]$ . It is worth noting that the calculation of  $\bar{\mathcal{F}}(\epsilon_\delta)$  is cleverly performed by introducing a set of Gaussian-type weights  $\omega_1, \omega_2, \dots, \omega_n$  with  $\sum_{i=1}^n \omega_i = 1$ , corresponding to a Gaussian sampling. Within an arbitrary noise range  $[-\epsilon_0, \epsilon_0]$ , we solve a large number of discrete fidelity numbers  $\mathcal{F}(\epsilon_{\delta i})$  alongside with a Gaussian-weighted random coefficient  $\omega_i$  which finally leads to a more realistic estimation for the average fidelity  $\bar{\mathcal{F}}(\epsilon_\delta)$ . Such setting of  $J_{der-i}$  leads to a tunable and noise-type-dependent weight  $\omega_i$  that can be easily applied to other noise sources.

The gate infidelity caused by residual thermal motion of atoms is revealed by calculating the relationship between  $\mathcal{F}(0) - \mathcal{F}(T)$  and the atomic temperature  $T$ , as plotted in Fig.3(a). To quantify the effect of Doppler effect, we compare the results by using the TO, DER, and DER-i pulses. We observe that the DER and DER-i pulses both benefit from a smaller dephasing error when the temperature is large outperforming the TO pulse. Inset of (a) gives a comparison of fidelity numbers under different  $\epsilon_\delta$  values which clearly confirms that the fidelity of the DER and DER-i pulses is counterintuitively

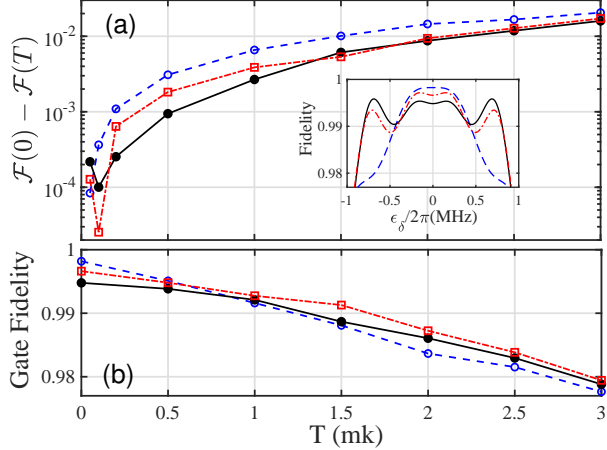


FIG. 3. (a) The gate infidelity of the TO(dashed-blue), DER(black), and DER-i(dash-dotted red) pulses in a wide parameter range of  $T \in [0, 3.0]$  mK. Inset: Fidelity versus detuning error  $\epsilon_\delta$  for the three pulses. (b) The realistic gate fidelity versus the temperature  $T$ . Here, the spontaneous decays from the intermediate state  $|p\rangle$  and the Rydberg state  $|r\rangle$  are considered, and other imperfections are not included. The optimal gate parameters for a DER-i pulse are  $(t_1, t_2, \omega) = (0.6508, 0.9053, 0.1627)$   $\mu\text{s}$ . Each point represents an average over 500 random samplings.

increased for larger detuning deviations. To show the gate performance in a more realistic condition, we calculate the gate fidelity by involving the effects of spontaneous decays( $|p\rangle, |r\rangle$ ) as well as a finite temperature, as display in Fig.3(b). When  $T < 0.5$  mK (corresponds to  $\epsilon_\delta/2\pi < 0.3048$  MHz), the DER and DER-i pulses have no advantages compared to the TO pulse, because the TO pulse is expected to perform best when the imperfection is small. However, as the temperature increases to  $T > 1.0$  mK we remark that the gate fidelity using the TO pulse is dramatically decreased, and the DER pulse shows a higher tolerance there. Moreover, associated with the consideration of Gaussian-type noise the DER-i gate also outperforms the other two gates in high temperatures. For a high-fidelity gate with  $\mathcal{F}$  staying over 0.99 the predicted atomic temperature can be as large as 1.5 mK (corresponds to  $\epsilon_\delta/2\pi \approx 0.5280$  MHz) using the DER-i pulse scheme. This requirement significantly relaxes the temperature constraint for trapped atoms in optical tweezers, greatly protecting the coherence in quantum gate operation from atomic temperature effect [73].

## B. Laser amplitude noise

We proceed by verifying the DER and DER-i pulses are also more robust against the laser amplitude noise. Amplitude fluctuations of the excitation lasers will not only affect the Rabi frequencies  $\Omega_p(t)$  and  $\Omega_c(t)$ , but also arise an extra two-photon detuning error  $\epsilon_\delta$ . Because,

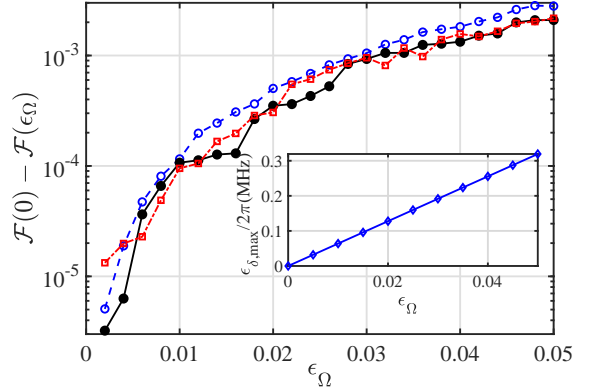


FIG. 4. The gate infidelity of the three pulses as a function of laser amplitude derivation  $\epsilon_\Omega$ . Here the DER-i pulse is re-optimized using a set of Uniform-type weights  $\omega_i$  (see Eq.18), resulting in the optimal gate parameters  $(t_1, t_2, \omega) = (0.6632, 0.9239, 0.1658)$   $\mu\text{s}$ . Note that for arbitrary  $\epsilon_\Omega$  the realistic laser amplitude noises  $\epsilon_{\Omega_p}, \epsilon_{\Omega_c}$  are random, independently extracted from  $[-\epsilon_\Omega, \epsilon_\Omega]$  by sufficient samplings ( $N=500$ ). Inset shows the relationship between the amplitude deviation  $\epsilon_\Omega$  and the maximal ac Stark shifts  $\epsilon_{\delta,\max}$  on the two-photon detuning. The linetype is same as in Fig.3.

typically the laser amplitude fluctuations [74] can result in an uncertainty in Rabi frequencies as

$$\Omega_p(t) \rightarrow \Omega_p(t)(1 + \epsilon_{\Omega_p}), \Omega_c(t) \rightarrow \Omega_c(t)(1 + \epsilon_{\Omega_c}) \quad (19)$$

For a two-photon transition system with a large intermediate detuning  $|\Delta_0| \gg \Omega_{p,c}$ , a significant ac Stark shift is revealed to the two-photon resonance  $\delta_{ac} = \frac{\Omega_c^2 - \Omega_p^2}{4\Delta_0}$  (remember  $\delta_0 = 0$ ), which evolves with time since  $\Omega_p(t), \Omega_c(t)$  are time-dependent [75]. While replacing by the fluctuated Rabi frequencies the realistic ac shift  $\delta_{ac}$  takes a more complex form as

$$\delta_{ac} = \delta_{ac,0} + \frac{\Omega_p^2}{2\Delta_0} \epsilon_{\Omega_p} - \frac{\Omega_c^2}{2\Delta_0} \epsilon_{\Omega_c} + \mathcal{O}(\epsilon_{\Omega_p}^2, \epsilon_{\Omega_c}^2) \quad (20)$$

where the known(first) term  $\delta_{ac,0}$  can be sufficiently compensated by a fixed detuning in experiment [76]. Nevertheless, the unknown (second and third) terms induce an unknown two-photon detuning error, which is

$$\epsilon_\delta = \frac{\Omega_p^2}{2\Delta_0} \epsilon_{\Omega_p} - \frac{\Omega_c^2}{2\Delta_0} \epsilon_{\Omega_c} \quad (21)$$

where we have ignored the higher-order terms. The maximal detuning deviation  $\epsilon_{\delta,\max}$  induced by ac Stark shifts is roughly calculated by  $\epsilon_{\delta,\max} = \max[\frac{\Omega_p^2 + \Omega_c^2}{2\Delta_0}] \times \epsilon_\Omega$  which is linear with the increase of  $\epsilon_\Omega$  as plotted in Fig.4(insert). For a large amplitude deviation  $\epsilon_\Omega = 0.05$ , the maximal detuning error is about  $2\pi \times 0.32$  MHz.

To quantify the robustness of different optimal pulses to the laser amplitude noise, Fig.4 shows the gate infidelity  $\mathcal{F}(0) - \mathcal{F}(\epsilon_\Omega)$  under different amplitude deviation

rates  $\epsilon_\Omega \in [0, 0.05]$ . Although the infidelity increases exponentially with  $\epsilon_\Omega$  for all three pulses, the DER and DER-i pulses benefit from a relatively smaller infidelity number as compared to the TO pulse, confirming the *active* robustness towards the laser amplitude noise by our new schemes. Because the amplitude deviation rate  $\epsilon_\Omega$  here, not only induces a laser amplitude noise that equally applies for the gate implementation, but also correlates an extra two-photon detuning error  $\epsilon_\delta$  from the ac Stark shift effect. So for any value of  $\epsilon_\Omega$  the robust pulses(DER, DER-i) always outperform the TO pulse for a smaller infidelity number. We also note that the DER-i pulse fails to outperform the DER pulse in this range because the induced detuning error  $\epsilon_{\delta, \max}/2\pi \leq 0.32$  MHz is still very small.

## VI. DISCUSSION AND SUMMARY

We present a scheme of high-fidelity adiabatic  $C_Z$  gates natively having *active* robustness to one type of errors, *i.e.*, the Rydberg two-photon detuning error. We mainly focus on optimizing the laser pulses to be insensitive towards the deviation of two-photon detuning, which may originate from versatile experimental imperfections, such as atomic temperature effect or laser amplitude noise. Based on the use of a cleverly-modified cost function that targets at minimizing the fluctuation of infidelity(average infidelity) in a certain error range, we observe the gate error due to Doppler shifts and laser amplitude deviations can be greatly suppressed, although at the expense of a slightly lower ideal fidelity. Additionally, the optimized laser pulse can be more effective by accounting for the type of error distributions. One example is when the DER-i pulse contains Gaussian-weighted coefficients in defining the average fidelity function  $\bar{\mathcal{F}}(\epsilon_\delta)$  it can outperform other two pulses (DER and TO) with an explicitly higher gate fidelity for larger atomic temperatures (Fig.3b). This work significantly relaxes the atomic temperature constraint in a Rydberg experiment by reducing the dephasing effect from atomic velocity and position fluctuations [77]. The new DER and DER-i pulses have more advantages when the experimental imperfections are large, *e.g.* a high temperature  $\sim$  mK, which enables the advanced atomic cooling or optical pumping techniques unnecessary for future experiments.

While we still admit that, our new pulses(DER and DER-i) do not explicitly have enhanced and *active* robustness to other noises as compared to the TO pulse, such as the intermediate detuning error, inhomogeneity in Rabi frequencies, laser phase noise and fluctuated interatomic interactions (see Appendix C). Especially the laser phase noise manifests as a time-dependent parameter fluctuation which contributes to the gate error at a comparable level as the laser amplitude noise [46, 64]. Finally we believe that, our results provide a more prospective method for achieving high-fidelity Rydberg gates, combining with the promising merits of *active* robust-

ness to any imperfection associated with the two-photon detuning deviation. An actively noise-robust pulse will inspire further experimental improvements focusing on the suppression of one type of errors for some important tasks in the field of large-scale quantum computation [78–81].

## ACKNOWLEDGMENTS

We acknowledge financial support from the National Natural Science Foundation of China under Grants No. 12174106, No. 11474094 and No. 11104076, by the Science and Technology Commission of Shanghai Municipality under Grant No.18ZR1412800.

## Appendix A: Effective dynamics for $C_Z$ gates

In this section, we demonstrate the physics associated with the implementation of a  $C_Z$  gate. We start with the single-atom frame described by a three-level non-fluctuated Hamiltonian in the  $\{|1\rangle, |p\rangle, |r\rangle\}$  basis

$$\hat{H} = \frac{\Omega_p}{2}|p\rangle\langle 1| + \frac{\Omega_c}{2}|r\rangle\langle p| + \text{H.c.} - \delta_0|r\rangle\langle r| - \Delta_0|p\rangle\langle p| \quad (\text{A1})$$

in which we use symbol  $\delta_0$  for a small two-photon detuning(note that  $\delta_0 = 0$  in the maintext). Due to the large detuning condition  $|\Delta_0| \gg \Omega_{p,c}, \delta_0$ , we can perform adiabatic elimination for state  $|p\rangle$  [82] which leads to the effective two-level dynamics, as

$$\hat{H}_{\text{eff}} = \frac{\tilde{\Omega}}{2}|r\rangle\langle 1| + \text{H.c.} + \frac{\Omega_p^2}{4\Delta_0}|1\rangle\langle 1| + (\delta_0 + \frac{\Omega_c^2}{4\Delta_0})|r\rangle\langle r| \quad (\text{A2})$$

where  $\tilde{\Omega} = \frac{\Omega_p\Omega_c}{2\Delta_0}$  is the effective Rabi frequency.

When the input state is  $|01\rangle$ (and  $|10\rangle$ ) with only one excited atom, the dynamics is given by the coupling of single atom, rewritten as

$$\hat{H}_{01} = \frac{\tilde{\Omega}}{2}|0r\rangle\langle 01| + \text{H.c.} + \delta'|0r\rangle\langle 0r| \quad (\text{A3})$$

with the two-photon detuning  $\delta' = \delta_0 + \delta_{ac} = \delta_0 + \frac{\Omega_c^2 - \Omega_p^2}{4\tilde{\Omega}}$ , forming a two-level system with Rabi frequency  $\tilde{\Omega}$  and detuning  $\delta'$ . Whereas it becomes a little more complicated for the  $|11\rangle$  state. There are six symmetric states  $\{|11\rangle, \frac{|1p\rangle+|p1\rangle}{\sqrt{2}}, |pp\rangle, \frac{|1r\rangle+|r1\rangle}{\sqrt{2}}, \frac{|pr\rangle+|rp\rangle}{\sqrt{2}}, |rr\rangle\}$  related to this problem. After adiabatic elimination of  $|p\rangle$  the initial Hamiltonian for the  $|11\rangle$  state is given by

$$\hat{H}_{11} = \hat{H}_{\text{eff}} \otimes \hat{I} + \hat{I} \otimes \hat{H}_{\text{eff}} + B|rr\rangle\langle rr| \quad (\text{A4})$$

which is equivalent to the matrix form in the  $\{|11\rangle, |\chi\rangle, |rr\rangle\}$  basis with  $|\chi\rangle = \frac{|1r\rangle+|r1\rangle}{\sqrt{2}}$ ,

$$\hat{H}_{11} = \begin{bmatrix} \frac{\Omega_p^2}{2\Delta_0} & \frac{\sqrt{2}\tilde{\Omega}}{2} & 0 \\ \frac{\sqrt{2}\tilde{\Omega}}{2} & \delta_0 + \frac{\Omega_c^2}{2\Delta_0} & \frac{\sqrt{2}\tilde{\Omega}}{2} \\ 0 & \frac{\sqrt{2}\tilde{\Omega}}{2} & 2(\delta_0 + \frac{\Omega_c^2}{4\Delta_0}) + B \end{bmatrix} \quad (\text{A5})$$

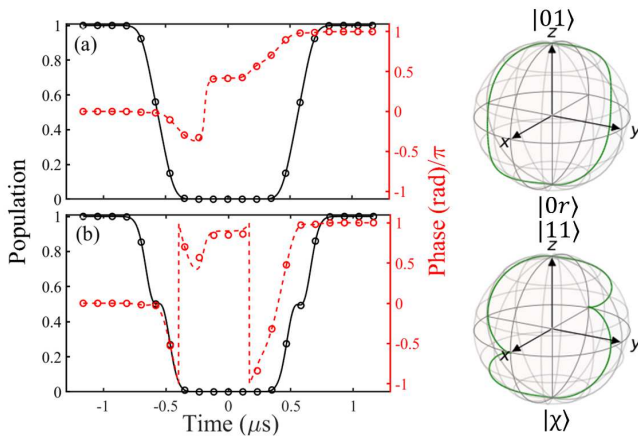


FIG. 5. The population dynamics and the phase evolution of states (a)  $|01\rangle$  and (b)  $|11\rangle$ . The population returns back with the accumulated phase  $\phi_{10} \approx 1.00000\pi$  and  $\phi_{11} \approx 0.99902\pi$ . For specific choice of the TO pulse  $2\phi_{01} - \phi_{11} \approx 1.00098\pi$ . Results based on the effective two-level systems(circles) have a perfect agreement with the original dynamics(lines).

After eliminating  $|rr\rangle$  within the Rydberg blockade regime, we arrive at an effective coupling between  $|11\rangle$  and  $|\chi\rangle$  as a similar two-level system

$$\hat{H}_{11} = \frac{\sqrt{2}\tilde{\Omega}}{2}|\chi\rangle\langle 11| + \text{H.c.} + \delta''|\chi\rangle\langle\chi| \quad (\text{A6})$$

with enhanced Rabi frequency  $\sqrt{2}\tilde{\Omega}$  and the detuning  $\delta'' = \delta' - \frac{\tilde{\Omega}^2}{\delta_0 + \frac{\Omega_c^2}{\Delta_0} + 2B}$ .

Taking the specific TO pulse as an example, we numerically confirm the implementation of a two-qubit  $C_Z$  gate by plotting the dynamical evolution of each basis state  $\{|01\rangle, |11\rangle\}$  combined with their accumulated phases, see Fig.5(a-b). Via the use of complete double STIRAP pulse sequences, both  $|01\rangle$  and  $|11\rangle$  return to their initial positions on the Bloch sphere at  $t = T_g$  forming an enclosed area [83]. For comparison the effective two-level dynamics is also calculated in the figure. Note that  $|00\rangle$  is uncoupled and therefore, accumulates no phase. State  $|01\rangle$  and  $|10\rangle$  are equivalent by symmetry so  $\phi_{01} = \phi_{10}$ . For the case of TO pulse we clearly see the population returning back to the desired state  $|01\rangle$  and  $|11\rangle$  after performing the double STIRAP pulse sequences in which the total phase accumulation  $\phi_{00} - \phi_{01} - \phi_{10} + \phi_{11} \approx -1.00098\pi$  realizes the  $C_Z$  gate.

## Appendix B: Cost function for the DER and DER-i pulses

We now turn to study the importance of a specifically-designed cost function. To find the robust pulse, we minimize the single cost function  $J_{der}$  using the Genetic optimization algorithm. The minimization of the first term

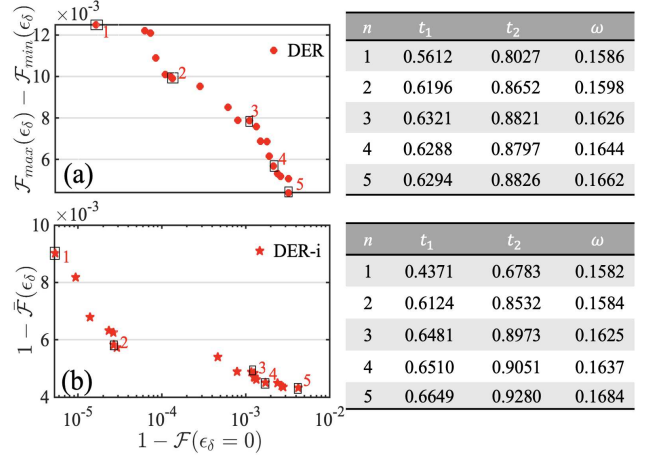


FIG. 6. Results from the multi-objective optimization for (a) DER and (b) DER-i cases. 20 Pareto points are given standing for a good trade-off between two objective functions. Tables on the right illustrate five representative pulse parameters  $(t_1, t_2, \omega)$  (in units of  $\mu\text{s}$ ), corresponding to the circled points in the figure.

$1 - \mathcal{F}(\epsilon_\delta = 0)$  is obtained when the ideal fidelity in the absence of any decay, is maximized. While the second terms  $\mathcal{F}_{\max}(\epsilon_\delta) - \mathcal{F}_{\min}(\epsilon_\delta)$  or  $1 - \bar{\mathcal{F}}(\epsilon_\delta)$  are contributed by minimizing the fluctuation of exact fidelity numbers in a certain error range  $[-\epsilon_0, \epsilon_0]$ . In the maintext, for a set of optimal pulse parameters  $(t_1, t_2, \omega)$ , the single cost function  $J_{der}$  or  $J_{der-i}$  can be minimized by comparing the competing effects from two terms treating as the way of single-objective optimization.

To show the competing effect of two terms, we introduce the results based on multi-objective optimization [84], where the cost functions are composed by

$$\begin{aligned} J_{der1} &= 1 - \mathcal{F}(\epsilon_\delta = 0) \\ J_{der2} &= \mathcal{F}_{\max}(\epsilon_\delta) - \mathcal{F}_{\min}(\epsilon_\delta) \end{aligned} \quad (\text{B1})$$

for the DER pulse, and by

$$\begin{aligned} J_{der1-i} &= 1 - \mathcal{F}(\epsilon_\delta = 0) \\ J_{der2-i} &= 1 - \bar{\mathcal{F}}(\epsilon_\delta) \end{aligned} \quad (\text{B2})$$

for the DER-i pulse. By utilizing the method of multi-objective function in the numerical Genetic algorithm, we find that, there is a very obvious competition between the two objective functions. This finding further confirms if we want to improve the pulse robustness, the fidelity at  $\epsilon_\delta = 0$ (ideal fidelity) needs to be sacrificed.

In the multi-objective optimization, we introduce the Pareto solution to find the most adaptive pulse parameters. By using  $J_{der1}(J_{der1-i})$  and  $J_{der2}(J_{der2-i})$  as two individual objective functions, we obtain a set of Pareto points [85] as displayed in Fig.6(a) and (b) which explicitly shows an inverse relationship between them. As expected, the suppression of fidelity sensitivity to experimental imperfections requires a larger sacrifice in the

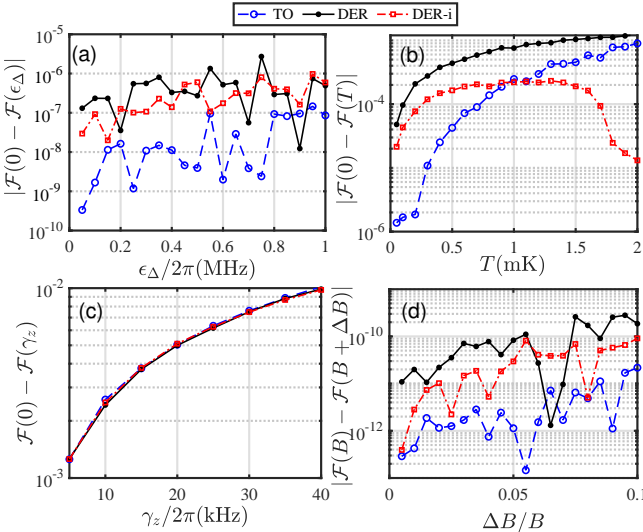


FIG. 7. The gate infidelity of the TO, DER, DER-i pulses caused by other error sources including (a) The detuning error due to intermediate-state detuning deviation  $\epsilon_\Delta$  (here  $\Delta_0/2\pi = 2.0$  GHz); (b) Inhomogeneous laser Rabi frequency coming from atom position fluctuations associated with the variation of temperature  $T$ ; (c) Average dephasing effect denoted by rate  $\gamma_z$  due to the time-dependent laser phase noise; (d) Random variations  $\Delta B$  in the non-fluctuated interatomic interaction  $B$ . Each point in all figures shows an average fidelity over 500 independent realizations.

ideal fidelity (for  $J_{der2-i} = 4.3 \times 10^{-3}$  the ideal fidelity lowers to 0.9958). Here each point presents a set of reasonable pulse parameters  $(t_1, t_2, \omega)$  as exemplified in the Table of Fig.6. Due to the competing effect the optimal pulse parameters used for implementing, the gate should satisfy a trade-off between two aspects: ideal fidelity and robustness.

### Appendix C: Passive influences by other noises

In order to characterize the gate performance in the presence of all experimental imperfections, in this section, we study other errors owing to the detuning deviation from the intermediate state  $|p\rangle$ , inhomogeneity in Rabi frequency, laser phase noise, as well as the Rydberg interaction fluctuations. We address that our robust gate is passively influenced by those errors so the DER(or DER-i) pulse does not have explicit robustness to them as compared with the TO pulse.

*Intermediate detuning error* - To assess the performance of gate in a fluctuated intermediate-state detuning  $\Delta_0 \rightarrow \Delta_0 + \epsilon_\Delta$ , we now study the infidelity with a randomly distributed error  $\epsilon_\Delta$ . In a realistic experiment, this intermediate detuning error is inevitable due to the laser frequency fluctuation or atomic temperature effect [86]. However since a large intermediate detuning  $|\Delta_0| \gg \Omega_{p,c}$  is set for a two-photon process; therefore,

$\epsilon_\Delta \ll |\Delta_0|$  which makes the detuning error negligible. We numerically verify the negligible effect of  $\epsilon_\Delta$  on the gate infidelity  $\mathcal{F}(0) - \mathcal{F}(\epsilon_\Delta)$  for all three pulses as shown in Fig.7(a). Note that the fluctuated detuning  $\Delta_0 + \epsilon_\Delta$  is also reversed to  $-(\Delta_0 + \epsilon_\Delta)$  halfway for cancelling the dynamical phase. It is clear that the infidelity caused by different  $\epsilon_\Delta$  values stays below  $10^{-6}$ . This is expected because the large intermediate detuning  $\Delta_0$  can efficiently suppress the intermediate population during the gate duration leading to a negligible error [87]. In addition we observe the TO pulse shows a relatively better robustness  $\sim 10^{-8}$  to the  $\epsilon_\Delta$  because of the presence of a perfect dark state  $|d\rangle$  (see Sec. III.A). While the DER or DER-i pulse is more robust for the deviation of  $\epsilon_\delta$ , not necessarily the most robust for the  $\epsilon_\Delta$ . Finally since  $\Delta_0$  is not an optimal value, we also observe the infidelity oscillations with respect to the change of  $\epsilon_\Delta$ .

*Inhomogeneous Rabi frequency* - In general the atom position fluctuations are inevitable in experiments which directly lead to a position-dependent laser Rabi frequency. Therefore the realistic Rabi frequency perceived by the atoms will deviate from its ideal value. According to Ref.[88], we replace  $\Omega_p(t)$  and  $\Omega_c(t)$  by position-dependent functions  $\Omega_p(\mathbf{r}, t)$  and  $\Omega_c(\mathbf{r}, t)$ , which are expressed as

$$\Omega_p(\mathbf{r}, t) = \Omega_p(0, t) \frac{e^{-\frac{x^2}{\omega_{x,p}^2(1+\frac{z^2}{L_{x,p}^2})}} - \frac{y^2}{\omega_{y,p}^2(1+\frac{z^2}{L_{y,p}^2})}}{[(1+\frac{z^2}{L_{x,p}^2})(1+\frac{z^2}{L_{y,p}^2})]^{1/4}} \quad (C1)$$

$$\Omega_c(\mathbf{r}, t) = \Omega_c(0, t) \frac{e^{-\frac{x^2}{\omega_{x,c}^2(1+\frac{z^2}{L_{x,c}^2})}} - \frac{y^2}{\omega_{y,c}^2(1+\frac{z^2}{L_{y,c}^2})}}{[(1+\frac{z^2}{L_{x,c}^2})(1+\frac{z^2}{L_{y,c}^2})]^{1/4}} \quad (C2)$$

where  $\Omega_{p,c}(0, t) = \Omega_{p,c}(t)$  is the originally optimized waveform and  $\mathbf{r} = (x, y, z)$  presents the atom position at any time  $t$  that satisfies a Gaussian distribution

$$f(\mathbf{r}) = \frac{1}{(2\pi)^{3/2}\sigma_x\sigma_y\sigma_z} e^{-\frac{x^2}{2\sigma_x^2}} e^{-\frac{y^2}{2\sigma_y^2}} e^{-\frac{z^2}{2\sigma_z^2}} \quad (C3)$$

When the laser waists are  $\omega_{x,p} = \omega_{y,p} = 7.8 \mu\text{m}$ ,  $\omega_{x,c} = \omega_{y,c} = 8.3 \mu\text{m}$ , arising the Rayleigh lengths  $L_{x(y),p} = 455.08 \mu\text{m}$ ,  $L_{x(y),c} = 213.65 \mu\text{m}$ , respectively for the 420 nm and 1013 nm lasers. The standard deviation  $\sigma_{x,y,z}$  in  $f(\mathbf{r})$  can be estimated by  $\sigma_{x,y,z} = \sqrt{k_B T / m \omega_{x,y,z}^2}$  with trapping frequencies  $\omega_{x,y,z}/2\pi = (147, 117, 35) \text{ kHz}$  chosen from [89], which arises the maximal uncertainty in the atom position  $(\sigma_x, \sigma_y, \sigma_z) = (0.47, 0.60, 1.99) \mu\text{m}$  at  $T = 2 \text{ mK}$ . That means the realistic deviation of Rabi frequency felt by atoms is still very small owing to  $\sigma_x \ll \omega_{x,p(c)}$ ,  $\sigma_y \ll \omega_{y,p(c)}$  even at a high temperature.

Our results are summarized in Fig.7(b) where the infidelity caused by inhomogeneous Rabi frequency varies with the atomic temperature  $T$ . We observe that, although the waist of a Gaussian laser can be adjustable

experimentally by using different incident angles, for a reasonable temperature, atoms in the optical traps can still be uniformly illuminated by both Rydberg excitation lasers [90]. Because the maximal deviation of atom position is smaller than the beam waist by orders of magnitude. From Fig.7(b) the robust pulses do not have explicit advantages against this inhomogeneity error and the DER and TO pulses reveal a similar trend of insensitivity. Here we note that the DER-i pulse shows an anomalous reduction in the gate infidelity achieving  $|\mathcal{F}(0) - \mathcal{F}(T)| \approx 1.31 \times 10^{-5}$  for  $T = 2$  mK. This is because the originally optimized pulse  $\Omega_{p,c}(0, t)$  is explicitly robust to the two-detuning error, but not the best to other errors such as the error induced by inhomogeneous Rabi frequency. Slightly shifting Rabi frequency via atom position can instead improve the gate insensitivity to the variation of temperature.

*Laser phase noise* - The Rydberg excitation lasers, not only have amplitude fluctuation as discussed in Sec.VB, but also contribute significant phase noise. Due to different frequencies involved in excitation lasers, the realistic Rabi frequency can be described by

$$\Omega_{p,c}(t) \rightarrow \Omega_{p,c}(t)e^{i\phi_{p,c}(t)} \quad (C4)$$

where  $\phi_{p,c}(t)$  presents a random phase typically featuring time-dependent fluctuations [64].

Accounting for the fact that the laser phase noise has shown its contribution to the decay of ground-Rydberg Rabi oscillations, it is reasonable to utilize a global dephasing model to quantify the average effect of laser phase noise as done by [91]. So here we newly introduce a Liouvillian dissipative operator  $\hat{\mathcal{L}}_z[\hat{\rho}]$ , serving as an extra non-Hermitian term in the master equation (8)

$$\hat{\mathcal{L}}_z[\hat{\rho}] = \sum_{l \in \{c,t\}} \sum_{i \in \{1,2\}} \hat{\mathcal{L}}_i^l \hat{\rho} \hat{\mathcal{L}}_i^{l\dagger} - \frac{1}{2} \{ \hat{\mathcal{L}}_i^{l\dagger} \hat{\mathcal{L}}_i^l, \hat{\rho} \} \quad (C5)$$

where

$$\begin{aligned} \hat{\mathcal{L}}_1^l &= \sqrt{\gamma_1/2}(|p\rangle\langle p| - |1\rangle\langle 1|) \\ \hat{\mathcal{L}}_2^l &= \sqrt{\gamma_2/2}(|r\rangle\langle r| - |p\rangle\langle p|) \end{aligned}$$

represent dephasings of the control and target atoms with individual rates  $\gamma_1, \gamma_2$  associated with the optical transitions of  $|p\rangle \rightarrow |1\rangle$  and  $|r\rangle \rightarrow |p\rangle$ , which are randomly obtained from the range of  $[0, \gamma_z]$ . Figure 7(c) shows the gate infidelity caused by the increase of  $\gamma_z$ . Due to the impact of laser phase noise we see all three cases reveal a similar trend with an exponential enhancement in the gate infidelity  $\mathcal{F}(0) - \mathcal{F}(\gamma_z)$ . When  $\gamma_z/2\pi = 40$  kHz we find the average infidelity even reaches  $\sim 10^{-2}$  after running 500 simulations.

*Fluctuation of Rydberg interaction* - Our scheme relies on the Rydberg-blockade mechanism that are robust to the fluctuation of interatomic interaction [92]. Under finite temperature, the atom position in a trap will lead to a fluctuation  $\Delta B$  in interaction strength deviating from its expected value  $B$ . While benefiting from a strong long-range interaction to suppress the excitation of  $|rr\rangle$ , we find the impact of interaction fluctuation is very small. As displayed in Fig.7(d), we calculate the infidelity of the three pulses by varying the ratio  $\Delta B/B$  in the range of  $[0, 0.1]$ . The real fluctuation is a random number obtained from  $[-\Delta B, \Delta B]$  for each realization. If  $\Delta B/B = 0.1 (B/2\pi = 2.0$  GHz), the relative position deviation between two atoms is about  $\delta r = r_0^7 \Delta B / (6C_6) \approx 45.83$  nm [93], estimated by the position-dependent interaction strength  $B = C_6 / r_0^6$  with  $C_6 = 862.69$  GHz  $\cdot$   $\mu\text{m}^6$  ( $70S_{1/2}$ ) and  $r_0 = 2.75$   $\mu\text{m}$  [94]. Here, the infidelity of all pulses keeps at a very low level  $10^{-12} \sim 10^{-10}$  offering a negligible impact on the gate operations.

To briefly conclude, our proposed gates are passively affected by these error sources unrelated to the two-photon detuning, among which the laser phase noise plays the most dominant role. Because the use of adiabatic pulses will cause a prolonged gate duration, increasing the damping of Rabi oscillations for the ground-Rydberg transition. To reduce this phase noise, we may increase the peak amplitude that restricts the timescale for the gate duration [95], utilize the adiabatic rapid passage approach with single optimized pulse for a direct single-photon transition [96, 97] or the superadiabatic protocols [98]. In experiment, low-noise laser sources or diode lasers filtered by higher-finesse optical cavities will further eliminate the laser phase error [21, 70].

---

[1] I. Bloch, Quantum coherence and entanglement with ultracold atoms in optical lattices, *Nature* **453**, 1016 (2008).

[2] T. D. Ladd, F. Jelezko, R. Laflamme, Y. Nakamura, C. Monroe, and J. L. O'Brien, Quantum computers, *Nature* **464**, 45 (2010).

[3] M. Saffman, T. G. Walker, and K. Mølmer, Quantum information with rydberg atoms, *Rev. Mod. Phys.* **82**, 2313 (2010).

[4] X.-F. Shi, Quantum logic and entanglement by neutral rydberg atoms: methods and fidelity, *Quantum Science and Technology* **7**, 023002 (2022).

[5] D. Bluvstein, S. J. Evered, A. A. Geim, S. H. Li, H. Zhou, T. Manovitz, S. Ebadi, M. Cain, M. Kalinowski, D. Hangleiter *et al.*, Logical quantum processor based on reconfigurable atom arrays, *Nature* **626**, 58 (2024).

[6] Y. Xu, J. Chu, J. Yuan, J. Qiu, Y. Zhou, L. Zhang, X. Tan, Y. Yu, S. Liu, J. Li, F. Yan, and D. Yu, High-fidelity, high-scalability two-qubit gate scheme for superconducting qubits, *Phys. Rev. Lett.* **125**, 240503 (2020).

[7] M.-Z. Ai, S. Li, Z. Hou, R. He, Z.-H. Qian, Z.-Y. Xue, J.-M. Cui, Y.-F. Huang, C.-F. Li, and G.-C. Guo, Ex-

perimental realization of nonadiabatic holonomic single-qubit quantum gates with optimal control in a trapped ion, *Phys. Rev. Appl.* **14**, 054062 (2020).

[8] V. Schäfer, C. Ballance, K. Thirumalai, L. Stephenson, T. Ballance, A. Steane, and D. Lucas, Fast quantum logic gates with trapped-ion qubits, *Nature* **555**, 75 (2018).

[9] B. B. Zhou, P. C. Jerger, V. O. Shkolnikov, F. J. Heremans, G. Burkard, and D. D. Awschalom, Holonomic quantum control by coherent optical excitation in diamond, *Phys. Rev. Lett.* **119**, 140503 (2017).

[10] Z. Zhu, T. Chen, X. Yang, J. Bian, Z.-Y. Xue, and X. Peng, Single-loop and composite-loop realization of nonadiabatic holonomic quantum gates in a decoherence-free subspace, *Phys. Rev. Appl.* **12**, 024024 (2019).

[11] Z. Fu, P. Xu, Y. Sun, Y.-Y. Liu, X.-D. He, X. Li, M. Liu, R.-B. Li, J. Wang, L. Liu, and M.-S. Zhan, High-fidelity entanglement of neutral atoms via a rydberg-mediated single-modulated-pulse controlled-phase gate, *Phys. Rev. A* **105**, 042430 (2022).

[12] S. J. Evered, D. Bluvstein, M. Kalinowski *et al.*, High-fidelity parallel entangling gates on a neutral atom quantum computer, *Nature* **622**, 268 (2023).

[13] Y. Sun, P. Xu, P.-X. Chen, and L. Liu, Controlled phase gate protocol for neutral atoms via off-resonant modulated driving, *Phys. Rev. Appl.* **13**, 024059 (2020).

[14] R. Li, S. Li, D. Yu, J. Qian, and W. Zhang, Optimal model for fewer-qubit cnot gates with rydberg atoms, *Phys. Rev. Appl.* **17**, 024014 (2022).

[15] T. H. Chang, T. N. Wang, H. H. Jen, and Y.-C. Chen, High-fidelity rydberg controlled-z gates with optimized pulses, *New Journal of Physics* **25**, 123007 (2023).

[16] F. Cesa and H. Pichler, Universal quantum computation in globally driven rydberg atom arrays, *Phys. Rev. Lett.* **131**, 170601 (2023).

[17] S. Ebadi, A. Keesling, M. Cain, T. T. Wang, H. Levine, D. Bluvstein, G. Semeghini, A. Omran, J.-G. Liu, R. Samajdar *et al.*, Quantum optimization of maximum independent set using rydberg atom arrays, *Science* **376**, 1209 (2022).

[18] P.-Y. Song, J.-F. Wei, P. Xu, L.-L. Yan, M. Feng, S.-L. Su, and G. Chen, Fast realization of high-fidelity nonadiabatic holonomic quantum gates with a time-optimal-control technique in rydberg atoms, *Phys. Rev. A* **109**, 022613 (2024).

[19] D. Jaksch, J. I. Cirac, P. Zoller, S. L. Rolston, R. Côté, and M. D. Lukin, Fast quantum gates for neutral atoms, *Phys. Rev. Lett.* **85**, 2208 (2000).

[20] T. Xia, X. L. Zhang, and M. Saffman, Analysis of a controlled phase gate using circular rydberg states, *Phys. Rev. A* **88**, 062337 (2013).

[21] Y. Liu, Y. Sun, Z. Fu, P. Xu, X. Wang, X. He, J. Wang, and M. Zhan, Infidelity induced by ground-rydberg decoherence of the control qubit in a two-qubit rydberg-blockade gate, *Phys. Rev. Appl.* **15**, 054020 (2021).

[22] X.-F. Shi, Fast, accurate, and realizable two-qubit entangling gates by quantum interference in detuned rabi cycles of rydberg atoms, *Phys. Rev. Appl.* **11**, 044035 (2019).

[23] C. J. Picken, R. Legaie, K. McDonnell, and J. D. Pritchard, Entanglement of neutral-atom qubits with long ground-rydberg coherence times, *Quantum Science and Technology*, **4**, 015011 (2018).

[24] A. Pagano, S. Weber, D. Jaschke, T. Pfau, F. Meinert, S. Montangero, and H. P. Büchler, Error budgeting for a controlled-phase gate with strontium-88 rydberg atoms, *Phys. Rev. Res.* **4**, 033019 (2022).

[25] Y. Zhao, Y. Ye, H.-L. Huang, Y. Zhang, and Wu, Realization of an error-correcting surface code with superconducting qubits, *Phys. Rev. Lett.* **129**, 030501 (2022).

[26] C. Ryan-Anderson, J. G. Bohnet, K. Lee, D. Gresh, and Hankin, Realization of real-time fault-tolerant quantum error correction, *Phys. Rev. X* **11**, 041058 (2021).

[27] L. Egan, D. M. Debroy, C. Noel, A. Risinger, D. Zhu, D. Biswas, M. Newman, M. Li, K. R. Brown, M. Cetina *et al.*, Fault-tolerant control of an error-corrected qubit, *Nature* **598**, 281 (2021).

[28] L. Postler, S. Heußen, I. Pogorelov, M. Rispler, T. Feldker, M. Meth, C. D. Marciniak, R. Stricker, M. Ringbauer, R. Blatt *et al.*, Demonstration of fault-tolerant universal quantum gate operations, *Nature* **605**, 675 (2022).

[29] M. H. Abobeih, Y. Wang, J. Randall, S. Loenen, C. E. Bradley, M. Markham, D. J. Twitchen, B. M. Terhal, and T. H. Taminiau, Fault-tolerant operation of a logical qubit in a diamond quantum processor, *Nature* **606**, 884 (2022).

[30] S. Krinner, N. Lacroix, A. Remm, A. Di Paolo, E. Genois, C. Leroux, C. Hellings, S. Lazar, F. Swiadek, J. Herrmann *et al.*, Realizing repeated quantum error correction in a distance-three surface code, *Nature* **605**, 669 (2022).

[31] U. Güngördü and J. P. Kestner, Robust quantum gates using smooth pulses and physics-informed neural networks, *Phys. Rev. Res.* **4**, 023155 (2022).

[32] C. Zhang, Y. Liu, J. Song, Y. Xia, and Z.-C. Shi, High-fidelity quantum gates via optimizing short pulse sequences in three-level systems, *New Journal of Physics* **26**, 013024 (2024).

[33] Z.-C. Shi, J.-T. Ding, Y.-H. Chen, J. Song, Y. Xia, X. Yi, and F. Nori, Supervised learning for robust quantum control in composite-pulse systems, *Phys. Rev. Appl.* **21**, 044012 (2024).

[34] S. Jandura and G. Pupillo, Time-optimal two-and three-qubit gates for rydberg atoms, *Quantum* **6**, 712 (2022).

[35] S. Jandura, J. D. Thompson, and G. Pupillo, Optimizing rydberg gates for logical-qubit performance, *PRX Quantum* **4**, 020336 (2023).

[36] H.-R. Noh and H. S. Moon, Transmittance signal in real ladder-type atoms, *Phys. Rev. A* **85**, 033817, (2012).

[37] T. Keating, R. L. Cook, A. M. Hankin, Y.-Y. Jau, G. W. Biedermann, and I. H. Deutsch, Robust quantum logic in neutral atoms via adiabatic rydberg dressing, *Phys. Rev. A* **91**, 012337 (2015).

[38] C. Fromont, D. Bluvstein, and H. Pichler, Protocols for rydberg entangling gates featuring robustness against quasistatic errors, *PRX Quantum* **4**, 020335 (2023).

[39] M. Saffman, I. I. Beterov, A. Dalal, E. J. Páez, and B. C. Sanders, Symmetric rydberg controlled-z gates with adiabatic pulses, *Phys. Rev. A* **101**, 062309 (2020).

[40] Y.-D. Wang, R. Zhang, X.-B. Yan, and S. Chesi, Optimization of stirap-based state transfer under dissipation, *New Journal of Physics* **19**, 093016 (2017).

[41] K. Blekos, D. Stefanatos, and E. Paspalakis, Performance of superadiabatic stimulated raman adiabatic passage in the presence of dissipation and ornstein-uhlenbeck dephasing, *Phys. Rev. A* **102**, 023715 (2020).

[42] A. Dalal and B. C. Sanders, Two-qubit gate in neutral atoms using transitionless quantum driving, *Phys. Rev.*

A **107**, 012605 (2023).

[43] J.-L. Wu, Y. Wang, J.-X. Han, S.-L. Su, Y. Xia, Y. Jiang, and J. Song, Resilient quantum gates on periodically driven rydberg atoms, Phys. Rev. A **103**, 012601 (2021).

[44] P. Bohlouli-Zanjani, J. A. Petrus, and J. D. D. Martin, Enhancement of rydberg atom interactions using ac stark shifts, Phys. Rev. Lett. **98**, 203005 (2007).

[45] K. M. Maller, M. T. Lichtman, T. Xia, Y. Sun, M. J. Piotrowicz, A. W. Carr, L. Isenhower, and M. Saffman, Rydberg-blockade controlled-not gate and entanglement in a two-dimensional array of neutral-atom qubits, Phys. Rev. A **92**, 022336 (2015).

[46] X. Jiang, J. Scott, M. Friesen, and M. Saffman, Sensitivity of quantum gate fidelity to laser phase and intensity noise, Phys. Rev. A **107**, 042611 (2023).

[47] X. Shao, F. Liu, X. Xue, W. Mu, and W. Li, High-fidelity interconversion between greenberger-horne-zeilinger and  $w$  states through floquet-lindblad engineering in rydberg atom arrays, Phys. Rev. Appl. **20**, 014014 (2023).

[48] C. Simonelli, M. Archimi, L. Asteria, D. Capecchi, G. Masella, E. Arimondo, D. Ciampini, and O. Morsch, Deexcitation spectroscopy of strongly interacting rydberg gases, Phys. Rev. A **96**, 043411 (2017).

[49] K.-N. Schymik, B. Ximenez, E. Bloch, D. Dreon, A. Signoles, F. Nogrette, D. Barredo, A. Browaeys, and T. Lahaye, In situ equalization of single-atom loading in large-scale optical tweezer arrays, Phys. Rev. A **106**, 022611 (2022).

[50] E. Urban, T. A. Johnson, T. Henage, L. Isenhower, D. Yavuz, T. Walker, and M. Saffman, Observation of rydberg blockade between two atoms, Nature Physics **5**, 110 (2009).

[51] A. Gaëtan, Y. Miroshnychenko, T. Wilk, A. Chotia, M. Viteau, D. Comparat, P. Pillet, A. Browaeys, and P. Grangier, Observation of collective excitation of two individual atoms in the rydberg blockade regime, Nature Physics **5**, 115 (2009).

[52] L. Béguin, A. Vernier, R. Chicireanu, T. Lahaye, and A. Browaeys, Direct measurement of the van der waals interaction between two rydberg atoms, Phys. Rev. Lett. **110**, 263201 (2013).

[53] P. R. Berman, H. Nguyen, and A. G. Rojo, Theory of the rydberg blockade with multiple intermediate-state excitations, Phys. Rev. A **105**, 043715 (2022).

[54] H. Levine, A. Keesling, G. Semeghini, A. Omran, T. T. Wang, S. Ebadi, H. Bernien, M. Greiner, V. Vuletić, H. Pichler, and M. D. Lukin, Parallel implementation of high-fidelity multiqubit gates with neutral atoms, Phys. Rev. Lett. **123**, 170503 (2019).

[55] L. P. Yatsenko, B. W. Shore, and K. Bergmann, Detrimental consequences of small rapid laser fluctuations on stimulated raman adiabatic passage, Phys. Rev. A **89**, 013831 (2014).

[56] I. I. Beterov, M. Saffman, E. A. Yakshina, V. P. Zhukov, D. B. Tretyakov, V. M. Entin, I. I. Ryabtsev, C. W. Mansell, C. MacCormick, S. Bergamini, and M. P. Fedoruk, Quantum gates in mesoscopic atomic ensembles based on adiabatic passage and rydberg blockade, Phys. Rev. A **88**, 010303 (2013).

[57] M. V. Berry, Quantal phase factors accompanying adiabatic changes, Proceedings of the Royal Society of London. A. Mathematical and Physical Sciences **392**, 45 (1984).

[58] D. Møller, L.B. Madsen, and K. Mølmer, Geometric phase gates based on stimulated raman adiabatic passage in tripod systems, Phys. Rev. A **75**, 062302 (2007).

[59] E. Braaten, H.-W. Hammer, and G. P. Lepage, Lindblad equation for the inelastic loss of ultracold atoms, Phys. Rev. A **95**, 012708 (2017).

[60] D. D. B. Rao and K. Mølmer, Robust rydberg-interaction gates with adiabatic passage, Phys. Rev. A **89**, 030301 (2014).

[61] I. Cong, H. Levine, A. Keesling, D. Bluvstein, S.-T. Wang, and M. D. Lukin, Hardware-efficient, fault-tolerant quantum computation with rydberg atoms, Phys. Rev. X **12**, 021049 (2022).

[62] R. Li, J. Qian, and W. Zhang, Proposal for practical rydberg quantum gates using a native two-photon excitation, Quantum Science and Technology **8**, 035032 (2023).

[63] D. Petrosyan, F. Motzoi, M. Saffman, and K. Mølmer, High-fidelity rydberg quantum gate via a two-atom dark state, Phys. Rev. A **96**, 042306 (2017).

[64] S. de Léséleuc, D. Barredo, V. Lienhard, A. Browaeys, and T. Lahaye, Analysis of imperfections in the coherent optical excitation of single atoms to rydberg states, Phys. Rev. A **97**, 053803 (2018).

[65] T. M. Graham, M. Kwon, B. Grinkemeyer, Z. Marra, X. Jiang, M. T. Lichtman, Y. Sun, M. Ebert, and M. Saffman, Rydberg-mediated entanglement in a two-dimensional neutral atom qubit array, Phys. Rev. Lett. **123**, 230501 (2019).

[66] C.-Y. Guo, L.-L. Yan, S. Zhang, S.-L. Su, and W. Li, Optimized geometric quantum computation with a mesoscopic ensemble of rydberg atoms, Phys. Rev. A **102**, 042607 (2020).

[67] X.-F. Shi and T. A. B. Kennedy, Annulled van der waals interaction and fast rydberg quantum gates, Phys. Rev. A **95**, 043429 (2017).

[68] J.-F. Wei, F.-Q. Guo, D.-Y. Wang, Y. Jia, L.-L. Yan, M. Feng, and S.-L. Su, Fast multiqubit rydberg geometric fan-out gates with optimal control technology, Phys. Rev. A **105**, 042404 (2022).

[69] H.-N. Wu, C. Zhang, J. Song, Y. Xia, and Z.-C. Shi, Composite pulses for optimal robust control in two-level systems, Phys. Rev. A **107**, 023103 (2023).

[70] H. Levine, A. Keesling, A. Omran, H. Bernien, S. Schwartz, A. S. Zibrov, M. Endres, M. Greiner, V. Vuletić, and M. D. Lukin, High-fidelity control and entanglement of rydberg-atom qubits, Phys. Rev. Lett. **121**, 123603 (2018).

[71] X.-F. Shi, Suppressing motional dephasing of ground-rydberg transition for high-fidelity quantum control with neutral atoms, Phys. Rev. Appl. **13**, 024008 (2020).

[72] M. Saffman and T. G. Walker, Analysis of a quantum logic device based on dipole-dipole interactions of optically trapped rydberg atoms, Phys. Rev. A **72**, 022347 (2005).

[73] X. Li, X. Shao, and W. Li, Single temporal-pulse-modulated parameterized controlled-phase gate for rydberg atoms, Phys. Rev. Appl. **18**, 044042, (2022).

[74] M. Mohan, R. de Keijzer, and S. Kokkelmans, Robust control and optimal rydberg states for neutral atom two-qubit gates, Phys. Rev. Res. **5**, 033052 (2023).

[75] P. G. Di Stefano, E. Paladino, A. D'Arrigo, and G. Falci, Population transfer in a lambda system induced by detunings, Phys. Rev. B **91**, 224506 (2015).

[76] K. McDonnell, L. F. Keary, and J. D. Pritchard, Demonstration of a quantum gate using electromagnetically in-

duced transparency, *Phys. Rev. Lett.* **129**, 200501 (2022).

[77] C.He and R.R. Jones, Active suppression of quantum dephasing in resonantly driven ensembles, *Phys. Rev. Lett.* **132**, 043201 (2024).

[78] Y. Wu, S. Kolkowitz, S. Puri, and J. D. Thompson, Erasure conversion for fault-tolerant quantum computing in alkaline earth rydberg atom arrays, *Nature communications* **13**, 4657 (2022).

[79] W.Sun, S.Bharadwaj, L.-P. Yang, Y.-L. Hsueh, Y.Wang, D.Jiao, R.Rahman, and Z.Jacob, Limits to quantum gate fidelity from near-field thermal and vacuum fluctuations, *Phys. Rev. Appl.* **19**, 064038 (2023).

[80] Z.-Y.Fang, H.Xu, T.Chen, K.Wei, and C.Zhang, Nonadiabatic geometric quantum gates by composite pulses based on superconducting qubits, *Phys. Rev. A* **109**, 042615 (2024).

[81] V. Crescimanna, J. Taylor, A. Z. Goldberg, and K. Heshami, Quantum control of rydberg atoms for mesoscopic quantum state and circuit preparation, *Phys. Rev. Appl.* **20**, 034019 (2023).

[82] M. M. Müller, M. Murphy, S. Montangero, T. Calarco, P. Grangier, and A. Browaeys, Implementation of an experimentally feasible controlled-phase gate on two blockaded rydberg atoms, *Phys. Rev. A* **89**, 032334 (2014).

[83] M. Tian, Z. W. Barber, J. A. Fischer, and W. R. Babbitt, Geometric manipulation of the quantum states of two-level atoms, *Phys. Rev. A* **69**, 050301 (2004).

[84] J. D. Schaffer, Multiple objective optimization with vector evaluated genetic algorithms, in *Proceedings of the first international conference on genetic algorithms and their applications*. (Psychology Press, 2014), pp. 93-100.

[85] R. Chakrabarti, R. Wu, and H. Rabitz, Quantum pareto optimal control, *Phys. Rev. A* **78**, 033414 (2008).

[86] G. S. Vasilev, A. Kuhn, and N. V. Vitanov, Optimum pulse shapes for stimulated raman adiabatic passage, *Phys. Rev. A* **80**, 013417 (2009).

[87] G. Pelegrí, A. J. Daley, and J. D. Pritchard, High-fidelity multiqubit rydberg gates via two-photon adiabatic rapid passage, *Quantum Science and Technology* **7**, 045020 (2022).

[88] X. L. Zhang, A. T. Gill, L. Isenhower, T. G. Walker, and M. Saffman, Fidelity of a rydberg-blockade quantum gate from simulated quantum process tomography, *Phys. Rev. A* **85**, 042310 (2012).

[89] Y. Chew, T. Tomita, T. P. Mahesh, S. Sugawa, S. de Léséleuc, and K. Ohmori, Ultrafast energy exchange between two single rydberg atoms on a nanosecond timescale, *Nature Photonics* **16**, 724 (2022).

[90] J. Zeiher, P. Schauß, S. Hild, T. Macrì, I. Bloch, and C. Gross, Microscopic characterization of scalable coherent rydberg superatoms, *Phys. Rev. X* **5**, 031015 (2015).

[91] H. Tamura, T. Yamakoshi, and K. Nakagawa, Analysis of coherent dynamics of a rydberg-atom quantum simulator, *Phys. Rev. A* **101**, 043421 (2020).

[92] X.-F. Shi, Rydberg quantum gates free from blockade error, *Phys. Rev. Appl.* **7**, 064017 (2017).

[93] H. Wang and J. Qian, Facilitation of controllable excitation in rydberg atomic ensembles, *Chinese Physics B* **32**, 083302 (2023).

[94] N. Šibalić, J. D. Pritchard, C. S. Adams, and K. J. Weatherill, Arc: An open-source library for calculating properties of alkali rydberg atoms, *Comput.Phys.Commun* **220**, 319 (2017).

[95] M. H. Goerz, E. J. Halperin, J. M. Aytac, C. P. Koch, and K. B. Whaley, Robustness of high-fidelity rydberg gates with single-site addressability, *Phys. Rev. A* **90**, 032329 (2014).

[96] I. I. Beterov, D. B. Tretyakov, V. M. Entin, E. A. Yakshina, I. I. Ryabtsev, M. Saffman, and S. Bergamini, Application of adiabatic passage in rydberg atomic ensembles for quantum information processing, *Journal of Physics B: Atomic, Molecular and Optical Physics* **53**, 182001 (2020).

[97] A. Mitra, M. J. Martin, G. W. Biedermann, A. M. Marino, P. M. Poggi, and I. H. Deutsch, Robust mølmer-sørensen gate for neutral atoms using rapid adiabatic rydberg dressing, *Phys. Rev. A* **101**, 030301 (2020).

[98] A. Vepsäläinen, S. Danilin, and G. S. Paraoanu, Superadiabatic population transfer in a three-level superconducting circuit, *Science Advances* **5**, eaau5999 (2019).